DNN-Based Lichen Mapping Using AVIRIS-NG Hyperspectral Imagery and UAV Images in a Rocky Canadian Shield Landscape

Shahab Jozdani[1], Dongmei Chen[1], Robert H. Fraser[2], Wenjun Chen[2]

[1]Department of Geography and Planing, Queen’s University, Kingston, Ontario, Canada – shahab.jozdani, chendm@queensu.ca
[2]Canada Centre for Remote Sensing, Natural Resources Canada, 560 Rochester Street, Ottawa, ON K1S 5K2, Canada – robert.fraser, wenjun.chen@canada.ca

Keywords: Remote sensing, lichen mapping, hyperspectral imagery, AVIRIS-NG, deep learning, DNN

Abstract

Forage lichen fractional cover mapping using multi-spectral remote sensing (RS) data is challenging, especially over rocky landscapes where there is a high spectral correlation between lichens and non-lichen features. Given this, it is deemed that the use of airborne or satellite hyperspectral imagery may improve lichen mapping. In this study, we report the first results of using AVIRIS-NG hyperspectral imagery and UAV images to estimate forage lichen fractional cover (*Cladonia* spp.) in a rocky Canadian shield landscape where non-lichen bright features were prevalent. To estimate forage lichen fractional cover, we conducted a regression approach based on deep multi-layer perceptron (MLP) models whose number of hidden layers and neurons were determined using exhaustive grid search procedures. The three MLP models were trained and tested on four scenarios with different hyperspectral compression AVIRIS-NG band images and WorldView-3 (WV3) data of three sites. Our experiments showed that mapping lichen fractional cover using the 5 m AVIRIS-NG surface reflectance imagery was more accurate (i.e., higher R2 and lower RMSE values) than the one using a 4-band WorldView-3 (WV3) image with a spatial resolution of 2 m in most cases.

1. Introduction

Lichens are an important indicator of environmental quality and biodiversity and food source for many caribou (Asta et al. 2002; Pinho et al. 2004; Joly K and Jandt 2007; Palmroos et al. 2023). Disturbances to lichens may alter caribou distributions, migration patterns, and possibly lead to their population declines (Joly et al. 2009). Monitoring forage lichens is, therefore, a crucial and challenging task over different ranges and over large-scale areas. Due to the advantage of RS data (e.g., relatively low cost and wide spatial coverage), previous studies have reported the successful use of different RS images for lichen-cover mapping (Kennedy et al. 2020, Fraser et al. 2021, He et al. 2021, Jozdani, et al. 2021a, 2021b, Richardson et al. 2021). Most of the classic studies on lichen mapping using RS data are based on vegetation indices (e.g., Normalized Difference Vegetation Index (NDVI)) and/or lichen-specific indices (e.g., Normalized Difference Lichen Index (NDLI)) (Nordberg 1998, Hansen et al. 2001, Nordberg and Allard 2002).

For example, in a study focusing on mountainous areas of Sweden (Nordberg and Allard 2002), the potential of RS was exploited for monitoring changes in lichen cover by calculating NDVI using Landsat TM data. However, due to the limitations of NDVI in properly differentiating lichens from non-lichen features, it turned out that lichen change detection was substantially affected by the spectral similarity of lichens to those of other land cover types. This finding was in line with the conclusion drawn earlier by Petzold and Goward (1988), in which the authors reported that NDVI (derived from Landsat TM imagery) may not be a reliable measure for estimating lichen-cover fraction as the values of this index may be misinterpreted as sparse green vascular plants. Théau and Duguay (2004) improved the mapping of lichen abundance using Landsat TM data by employing Spectral Mixing Analysis (SMA), which is commonly used for extracting endmembers from hyperspectral images. In this respect, the authors selected lichen (*Cladina stellaris*), canopy (*Picea mariana*), and shadow as endmembers in the SMA to estimate the fraction of lichen cover that fell within each individual TM pixel over the study area. The authors reported that the SMA was able to correctly detect 79.7% of lichen-covered sites, although the SMA did not show a consistent behaviour over its lower and upper bounds of its values. In a more recent study, Falldorf et al. (2014) developed a lichen volume estimator (LVE) by training a 2D Gaussian regression model based on NDLI and Normalized Difference Moisture Index (NDMI) derived from Landsat TM images. Using a 10-fold cross-validation, the authors reported that the model achieved an R2 of 0.67. However, statistical assumptions in parametric models may not hold in different areas, and thus the model can fail to generalize.

Since the coarse spectral and spatial resolutions of publicly available optical/thermal data (such as Landsat and Sentinel-2 images) are an important barrier to reaching accurate lichen maps, recent endeavours in this field have primarily focused on improving the results through utilizing multi-scale and source data and more advanced, ML-based classification/regression approaches. In a study carried out by Macander et al. (2020), a multi-scale framework was proposed for mapping the fraction of lichen cover. The framework was based on utilizing multiple sources of images (i.e., micro-plot field data, UAV images, and Landsat imagery) to map lichen fractional cover using a Random Forest (RF) regression model. The authors reported that the model reached an R2 of 0.77 over the study area, although the model faced cases of under- and over-estimations of lichen fractional cover.

The use of a multi-scale approach for lichen fractional cover mapping was also considered in a recent study by He et al. (2021) where the authors presented a pipeline using neural networks to scale-up UAV-derived lichen maps to Landsat-8 imagery. In addition to the use of UAV and Landsat-8 images, the authors used an intermediate source of RS imagery (WorldView-2 (WV2) imagery) to increase the size of the training data that would then help improve the scale-up task. The authors' experiments showed that the proposed workflow achieved R2 values between 0.49 and 0.79.

In another study on improving the robustness of models for lichen mapping, Jozdani, et al. (2021a) investigated the potential of a semi-supervised approach to map lichen cover (i.e., binary classification) in high-resolution satellite imagery (WV2) in cases where very limited labelled data are available, which is a common problem in the context of RS. In fact, since the scale-up process in many cases starts from a small-scale UAV image, it limits the number of training data that can be used for the scale-up task, and thus true lichen pixels cannot be accurately detected at the satellite level (in this case, high-resolution satellite imagery). The authors found that involving unlabelled data in the training process led to a more robust/accurate model compared to using a fully supervised model, without collecting additional labelled data or further fine-tuning the model.

In a later study, Jozdani, et al. (2021b) considered another aspect of the lack of model robustness in lichen mapping caused by scene-to-scene illumination/lighting variations in non-atmospherically corrected RS images. For this purpose, the authors analysed the potential of conditional Generative Adversarial Networks (cGANs) to normalize target images to a source image on which the lichen detector model was trained. The authors reported that without any further training of the lichen detector model, it was possible to produce reasonably accurate lichen maps (F1-score of 75% to 91%) based on the cGAN-derived normalized target images.

The application of advanced approaches for lichen mapping was also reported in a recent study by Kennedy et al. (2020) in which a residual-based multi-layer perceptron (MLP) regression model was used to map lichen fractions. According to the experiments conducted in that study, the MLP regression model was overall superior to a Random Forest (RF) approach for lichen fractional cover mapping.

Recent advances in computer vision and machine learning have facilitated the way lichen maps can be produced automatically and less subjectively (Théau and Duguay 2004, Zhang et al. 2005, Gilichinsky et al. 2011, Falldorf et al. 2014, Macander et al. 2020). Although the potential of conventional machine learning algorithms like RF in environmental RS has been proven before (Belgiu and Drăguţ 2016), there is a wide range of papers achieving state-of-the-art accuracies based on deep learning (Ma et al. 2019, Yuan et al. 2020, Jozdani et al. 2022). Deep learning models have also been used in the field of lichen mapping (He et al. 2021, Jozdani et al. 2021a, 2021b, Pouliot et al. 2021, Richardson et al. 2021, 2023, Amarasingam et al. 2025) in recent years.

In a relevant study conducted by Fraser et al. (2021) on the importance of the spatial resolution of RS imagery, the authors utilized WorldView-3 (WV3) and UAV images to map forage lichen fractional cover in three rocky sites. In order to investigate the potential benefit of using higher spatial resolution satellite imagery for lichen mapping, the authors analyzed WV3 imagery with two different spatial resolutions in their experiments: 1) The original 2-m multi-spectral bands; and 2) the downscaled 6-m multi-spectral bands. Then, the authors compared the 2-m WV3 image with the downscaled 6-m one (along with the UAV image) to analyze the effect of downscaling on mapping lichen fractional cover over the three sites. The authors found that downscaling the WV3 image to 6-m helped them achieve more accurate forage lichen-cover fractions (i.e., higher R2 and lower RMSE values) over their rocky study area. This accuracy improvement when using coarser resolutions can be mainly ascribed to the variance reduction of both the dependent and independent variables used in an RF regression model (Riihimäki et al. 2019, Fraser et al. 2021).

Although it is deemed that the use of hyperspectral imagery can be advantageous for lichen mapping (Nordberg and Allard 2002), there is a lack of research on reporting the potential of utilizing such imagery for caribou lichen mapping over rocky landscapes owing to the scarcity of airborne and satellite hyperspectral data. Due to this issue, past research on the use of hyperspectral imagery for lichen mapping has been mainly based on terrestrial hyperspectral data that are not usable for large-area lichen mapping (Ager and Milton 1987, Petzold and Goward 1988). In this research, we focus on investigating the potential of using airborne hyperspectral imagery (AVIRIS-NG) and UAV images to map forage lichen fractional cover (Cladonia spp.) over three rocky sites (Fraser et al. 2021). We present the results obtained from conducting different tests to analyze the importance of employing a much higher spectral-resolution imagery (AVIRIS-NG) for lichen fractional cover mapping over a rocky landscape. In addition, by considering a high-resolution satellite image (WV3), we compared the importance of spatial resolution with spectral resolution for lichen fractional cover mapping. To handle the complexity of the RS data and landscape optimally, deep learning regression models were deployed in this study.

2. Methodology

2.1 Data and preprocessing

The study area for this research was located near Yellowknife, Northwest Territories, Canada (Figure 1). This area is covered by bedrocks and closed canopy forests consisting of aspen, paper birch, jack pine, and spruce and open lichen woodlands. UAV surveys were conducted over three sites (hereafter, they are referred to as S1, S2, S3 images/sites) from August 16 to 19, 2019. Within these three sites, Caledonia lichen (mainly Cladonia stellaris and Cladonia rangiferina) was the dominant forge lichen species. Bedrocks are mainly white to light pink Prosperous Granites (biotite-muscovite monzogranite to granodiorite), which are spectrally similar to Cladonia lichen.

Two different cameras were used in the UAV surveys: 1) 3.2 MP MicaSense Altum multispectral camera with 5 bands (RGB, NIR, Red Edge, and Thermal); and 2) Integrated 20-MP RGB CMOS sensor mounted on DIJ Phantom 4 RTK. The spatial resolution of the images acquired by the Altum camera was 3.2 cm, and that of the image acquired by the Phantom camera was 0.2 cm. The 0.2-cm Phantom images were used to collect training samples as they corresponded to the location of our field quadrats (with an area of ~0.1 ha). A total of 33 (11 quadrates for each UAV site) 50 cm × 50 cm quadrates were collected over the three UAV sites, although 8 of the quadrates were excluded due to significant nearby tree shadows. Orthomosaic Altum UAV images were generated using Pix4dmapper software. We used 5-m AVIRIS-NG airborne hyperspectral surface reflectance imagery acquired by NASA's Arctic-Boreal Vulnerability Experiment (Miller et al. 2018) on

https://doi.org/10.5194/isprs-archives-XLIX-B3-2026-1231-2026

August 7, 2017 over our study area. AVIRIS-NG imagery contains 425 spectral bands with a 5 nm interval in the visible to shortwave infrared spectrum. In addition, a 4-band (RGB-NIR) WorldView-3 image acquired on July 21, 2015, was used in this research. Although there is a 4-year gap between the UAV and WV3 acquisitions, and a 2-year gap between the UAV and AVIRIS-NG acquisitions, the areas have not dramatically changed over the past few years (i.e., short- and long-term disturbances did not have any significant impact on the forage lichen cover over the study area), and thus the images properly correspond to each other in terms of the underlying land-cover structure.

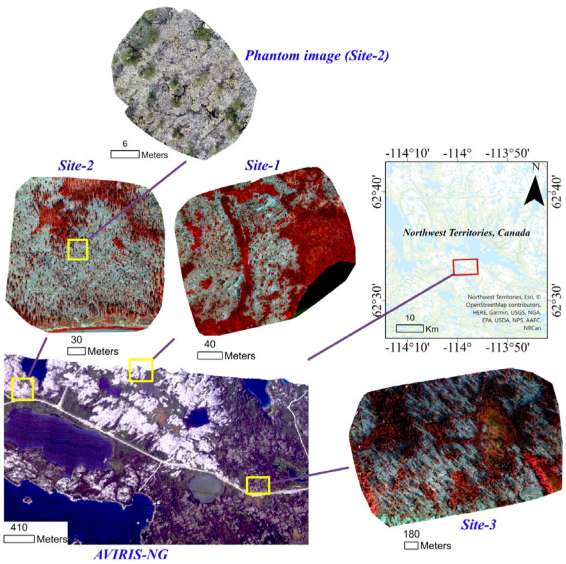

Figure 1. UAV and AVIRIS-NG images used in this study. Note: AVIRIS-NG Natural color composite = (R: band 54, G: band 36, B: band 20); Altum false color composite = NIR, Red, Blue; Phantom true color composite. The spatial resolution of the Altum images is 3.2 cm, whereas that of the Phantom image is 0.2 cm.

To co-register the three image sources, we first co-registered the WV3 image to the respective UAV orthomosaics and then co-registered the AVIRIS image to the co-registered WV3 image, indirectly leading to the co-registration of the UAV and AVIRIS images. This was because the direct co-registration of the AVIRIS image to the UAV image was not accurate due to the small extent of the UAV images and the significant difference between the spatial resolutions of the two image sources. The co-registrations were performed using the AROSICS tool, which is an open-source tool for automatically co-registering RS images (Scheffler et al. 2017). Noisy bands were removed from the AVIRIS-NG imagery based on the metadata and visual inspection, resulting in a total of 367 bands. The UAV images acquired over S2 and S3 sites are fully within the valid extent of the AVIRIS-NG image. However, only a little more than half of the S1 image fell within the AVIRIS-NG extent (Figure 1) (Fraser et al. 2021).

2.2 UAV reference data and classification

In order to estimate lichen percentage within each pixel footprint of AVIRIS-NG imagery, we first classified the three Altum UAV images as described in (Fraser et al. 2021). This involved collecting a total of 1710 training samples, of which 425 belonged to the “Cladonia lichen” class, and the rest to the other land cover types (including concentric ring lichen, bare rock, dark lichen (or smooth rock tripe), green vegetation, and shadow). These training samples were used to train an RF classifier with 100 trees. For each tree, 2/3rd of samples was randomly used with a square root of the number of features (i.e., 5 spectral bands, NDVI, Normalized Difference Red Edge (NDRE), and two Grey-Level Co-occurrence Matrix texture measures (Mean and Contrast) computed from a kernel size of 7-by-7 of the blue channel) as inputs to each tree. To test the accuracy of the classification, 400 samples were independently collected with equally sized lichen and non-lichen samples. All the training and test samples were delineated using the 0.2-cm Phantom image (Figure 1).

2.3 Deep-learning-based regression modelling

A regression modelling approach was used to estimate lichen fractional coverage in the AVIRIS-NG and WV3 images. Since past related research has shown the performance superiority of deep learning over conventional regression models (Kennedy et al. 2020), a multi-layer perceptron (MLP) approach was trained on each of the three sites. An MLP is composed of a series of fully connected layers that, given its depth, is able to model complex patterns in data and that has been widely used in different RS applications (Jozdani et al. 2019). To train the models, the Adam optimizer with a learning rate of 0.001 was employed. ReLU activation was used for all the layers except the output layer for which Sigmoid was used. Batch Normalization was also used before each activation layer to improve the robustness of the models. In order to set the number of hidden layers, the number of neurons, and dropout probability, we used a Bayesian hyperparameter tuning approach in PyTorch Ray Tune. In this regard, the number of layers ranged from 2 to 8), the number of neurons ranged from 10 to 500 with an interval of 10; all the layers were set to have the same number of neurons, and dropout tested with two values 0.25 and 0.5. The model that led to the highest accuracy on the validation set was used to perform testing (the hyperparameters selected can be seen in Table 1).

Table 1. Hyperparameters of the 12 MLP models selected through a Bayesian hyperparameter tuning approach.

Scenario	Model	# of hidden layers	# of neurons in each hidden layer	Dropout probability
AB	S1	4	300	0.25
	S2	8	300	0.25
	S3	8	430	0.25
PCA	S1	3	70	0.25
	S2	3	70	0.50
	S3	8	50	0.25
RFE	S1	3	200	0.50
	S2	3	180	0.25
	S3	5	150	0.50
WV3	S1	3	20	0.25
	S2	4	20	0.25
	S3	4	20	0.25

One of the main challenges when working with hyperspectral data is the potential correlations of their spectral bands. Rather than processing all the bands (AB), we performed two methods to select only a subset of bands that would be less correlated and more discriminative: Principal Component Analysis (PCA) and Recursive Feature Elimination (RFE). For the RFE approach, we applied an RF model (hereafter, RF-RFE) with 500 trees and the Mean Squared Error (MSE) metric to choose the band combinations that led to the lowest MSE value. To choose the most suitable first number of the components of the PCA data, an automatic approach was used by consecutively considering the first “N” bands and tests which “N” will lead to suitable accuracies. the RF model (hereafter, RF-PCA) with 500 trees (starting with the first two components) iteratively added the next component until either no significant accuracy improvement was achieved or accuracy dropped. This approach to reducing the dimensionality of the data were performed by pooling all three image sites together. This way, we could determine which bands/features and which number of first PCA components would be, on average, more suitable to proceed with rather than using all the 367 bands.

For all the AB, PCA, and RFE scenarios, a separate MLP model was trained on each of the three sites. The advantage of using MLPs over conventional models like RF for lichen fractional cover mapping has also recently been proven (Kennedy et al. 2020). We used 60% of the data of each site for training, 20% for validation (used for hyperparameter tuning in the grid search setup), and 20% for testing. After training each model on the three sites, it was applied to the 20% hold-out test data of the same image on which it was trained and to the other two images (i.e., all the data on the other two images were used for testing). This was done for all three images separately, resulting in a total number of 9 tests for each of the AB, PCA, and RFE scenarios.

3. Results

Our accuracy assessment results showed that the overall accuracies of classifying the Altum S1, S2, S3 UAV images were 97.5%, 96.2%, and 92.8%, respectively. Figure 2 shows the distribution of AVIRIS-NG pixels with respect to their lichen fractional cover. (Note that the highest lichen coverage within the AVIRIS-NG footprint was 59%). In this figure, for the sake of visual simplicity, we classified lichen fractions into 6 intervals (0-10%, 11-20%, 21-30%, 31-40%, 41-50%, and 51-60%). Apparently, lichen coverages within the 51-60% range were challenging to map as they were expected to have a higher mean reflectance than the other lichen coverage ranges. In fact, the mean reflectance values of this lichen cover range were lower than those of lower-cover ranges. Another challenging factor also visible in Figure 2 was that the three lichen coverages of 21-30%, 31-40%, and 41-50% have very similar distributions to each other. These two problems can also be seen in the signatures of these ranges as shown in Figure 3, which proves the complexity of lichen mapping over the study areas. In fact, these confusions in spectral signatures are the main reason that make differentiating lichens from rocks a very challenging task for machine learning models if sufficient spatial and spectral information is not provided during training.

In Figure 4, the first two components of the PCA-transformed data along with all the pooled data with their corresponding lichen fractional values are presented. Based on this figure, it is visible that apart from a portion of the smallest lichen fraction range (i.e., 0-10%), all the other ranges are not easily differentiable.

Based on the hyperparameter tuning conducted in this research (Table 1), the best models had at least 3 hidden layers and 20 neurons (for the WV3 S1 model). The deepest model had 8 hidden layers and 430 neurons (for the AB S3 model). Deeper models (more than 8 hidden layers) either did not improve the results or resulted in overfitting, deteriorating validation accuracy/loss. The depth of the models was a function of the number of data and the complexity of the patterns in the data used.

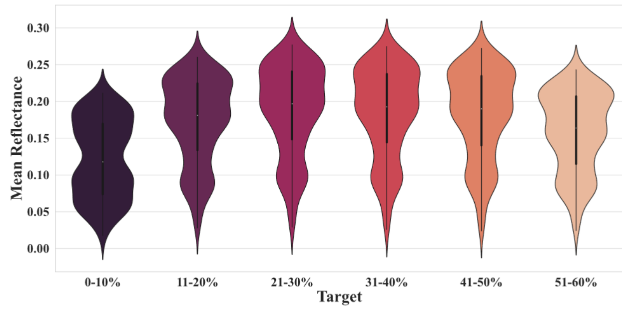

Figure 2. Violin plots showing the distributions of the six ranges of forage lichen fractions based on the pooled AVIRIS-NG data. The plots present both the distributions and statistics of different lichen fraction classes over the tree study sites.

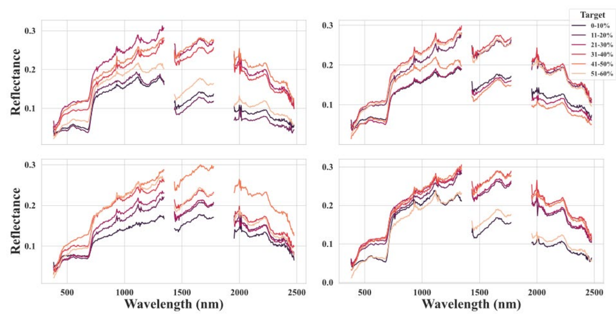

Figure 3. Spectral signatures of four groups of pixels for the six lichen fraction ranges based on the AVIRIS-NG imagery. Note: Each of the plots contains 6 different pixels that are representative of the six respective forage lichen fractional cover ranges.

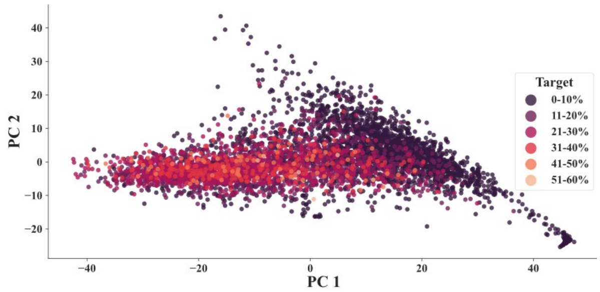

Figure 4. Visualization of the first two components of the PCA with respect to the six lichen fraction classes. As shown, using only the first two components, it is not possible to accurately estimate different lichen-cover fractions in AVIRIS-NG imagery.

The R2 and RMSE values of the regression models trained on the AVIRIS-NG image are presented in Figure 5 and Table 2. The performances of the regression models trained based on AB, PCA, and RFE were almost similar, highlighting that not all the bands of the hyperspectral image were needed to generate effective models. For the AB scenario, it is clear that the S1 model performed poorly on the other two images (R2 = 0.269 and 0.210; RMSE = 9.9% and 8.5% for S2 and S3 test images, respectively). In contrast, the S2 model generalized better on the S1 (R2 = 0.345; RMSE = 7.6%) and S3 (R2 = 0.344; RMSE = 7.7%) images than the other two models did on the respective test images.

Table 2. Assessment of regressions models of AB, PCA, RFE, and WV3 with R^2 and RMSE

Model		S1 test image	S2 test image	S3 test image
AB	S1 model	0.694	0.269	0.210
		5.3%	9.9%	8.5%
	S2 model	0.345	0.531	0.344
		7.6%	7.9%	7.7%
	S3 model	0.309	0.242	0.361
		7.8%	10.1%	6.9%
PCA	S1 model	0.682	0.357	0.231
		5.48%	9.3%	8.4%
	S2 model	0.393	0.540	0.370
		7.4%	7.8%	7.6%
	S3 model	0.248	0.269	0.305
		8.2%	9.9%	7.2%
RFE	S1 model	0.667	0.325	0.165
		5.6%	9.5%	8.7%
	S2 model	0.410	0.544	0.302
		7.2%	7.8%	8.0%
	S3 model	0.310	0.325	0.360
		7.8%	9.5%	6.9%
WV3	S1 model	0.497	0.116	0.362
		8.6%	14.6%	9.8%
	S2 model	0.235	0.352	0.402
		10.5%	12.4%	9.5%
	S3 model	0.149	0.104	0.416
		11.1%	14.7%	9.4%

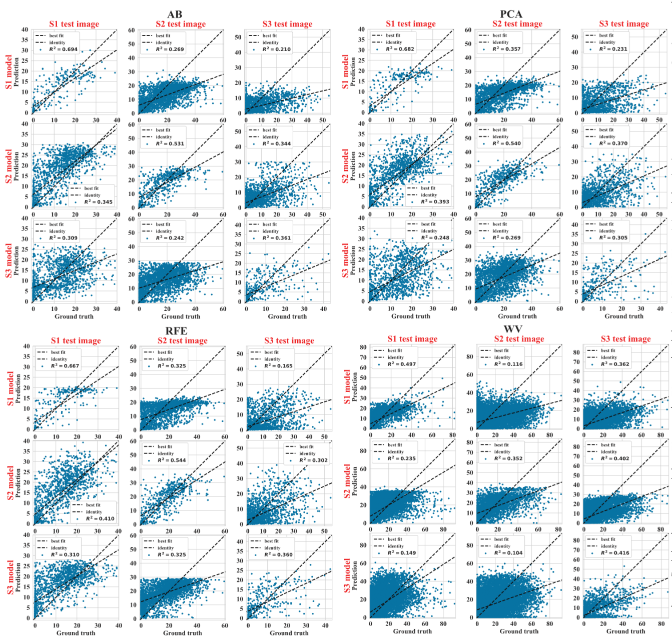

Figure 5. Prediction plots resulting from the models trained based on all bands (AB) of AVIRIS-NG, Principal Component Analysis (PCA), Recursive Feature Elimination (RFE), and WorldView-3 (WV3) scenarios for the three sites.

Performing the PCA on the pooled data, we observed that the first two components of the projected image explained more than 95% of the variance in the data. However, the complexity of the data for regression modeling was beyond the use of only the first two bands (Fig. 5) as the use of only the first two components resulted in poor accuracies due to the lack of representative features. To choose an appropriate number of the first components, the RF-PCA model found the 20 first components of the PCA data to be suitable for regression modeling. Using these 20 first components, we trained the models. The PCA-based regression models performed almost similar to the AB models. The most tangible differences, however, were for the S2 model with which a better generalization on S1 (R2 = 0.393; RMSE = 7.4%) and S3 images (R2 = 0.370; RMSE = 7.6%) was achieved, and for the S1 model that led to a better generalization on the S2 (R2 = 0.357; RMSE = 9.3%) and S3 (R2 = 0.231; RMSE = 8.4%) test images.

Applying the RF-RFE model resulted in the selection of a combination of 100 AVIRIS-NG bands as the most suitable number and combination to use in the MLP models. The performances of the S1 and S2 models in the RFE case were close to the models in AB and PCA. However, the S3 model of the RFE overall generated more accurate lichen-cover fractions than that of the AB and PCA. In fact, the S3 model of the RFE generalized better to the other two sites than the S3 models of the AB and PCA did.

The differences between the models trained on the respective WV3 and AVIRIS-NG images were significant in most of the cases. In most of the models, the regression models trained based on the AVIRIS-NG image performed better than those trained based on the WV3 image. In some cases (e.g., S3 model on S1 and S2 test images), the models based on the AVIRIS-NG image achieved much higher R2 (almost two times higher) and smaller RMSE (> 3%) values. In general, it is apparent that the models trained based on the WV3 image were able to better generalize better to the S3 image in terms of R2 although they, on average, led to higher RMSE values.

4. Discussions

In the previous section, the results of applying the regression models and their generalization performances on the three test images were provided. Overall, there is no single model standing out with the best performance in all test images. To some degree, it was expectable as the study area was a complex landscape where non-forage lichen bright features, especially rocks and concentric ring lichen, were widely present. Due to this complexity, we hypothesized that the many additional spectral bands provided by the AVIRIS-NG image would be beneficial to improve lichen fractional cover mapping over the study area. Our results confirmed this hypothesis by producing more accurate lichen fraction estimations.

According to the experiments, we found that S1 and S2 regression models did not generalize well on the S3 test image. The S3 image is generally a more complex image than the other two images, and it contains a different background of darker, sedimentary rock compared to the brighter granites encountered at sites 1 and 2 (Fraser et al. 2021). In fact, one important challenge with this image arose from the prevalence of shadows in this image that negatively affected the quality of the classification of this UAV image, as was also reflected in its lower classification accuracy compared to the two other sites (92.8% vs 97.5% and 96.2%). Another important challenge with this image was that the quality of co-registration of this image to AVIRIS-NG image was visually lower than the other two UAV sites. In contrast, the S3 WV3 image led to a higher quality co-registration than the S3 AVIRIS-NG image did, resulting in better generalization of the S1 and S2 WV3 models on the S3 WV3 image. Since the S1 image was a smaller site (because only a little more than half of it was covered by the AVIRIS-NG imagery), it was a simpler case for the S2 and S3 models to which they generalize well. In other words, both the S2 and S3 models generalized best on the S1 image in the AVIRIS-NG. Although the WV3 image was better co-registered to the UAV images than the AVIRIS-NG image did, we can see that it was not sufficient to obtain more accurate lichen-cover fractions using WV3 models compared to the AVIRIS-NG models. Despite its higher spatial resolution (which is could result in less mixed pixels), the WV3-based models suffered from the lack of sufficient discriminative features (i.e., spectral information) to improve lichen fractional mapping.

All the three scenarios (AB, PCA, and RFE) used to train the MLP models on AVIRIS-NG imagery resulted in almost similar lichen estimations. However, considering the efficiency of these approaches, we observed that the PCA models were generally more efficient, although they performed worse than their AB and RFE counterparts in some cases.

Notwithstanding the fact that the regression models based on the AVIRIS-NG image led to more accurate *Cladonia* lichen-cover fractions in most cases, they are still not as accurate as models trained on the downscaled (6 m) WV3 images over the same area in (Fraser et al. 2021). As discussed earlier, misclassification errors of the UAV images, co-registration errors, complexity of the area, and noise in the AVIRIS-NG imagery are the main causes of these low accuracy estimates. Of the above factors, we were able to limit the UAV misclassification errors to a large degree. Co-registration errors were, however, more difficult to address. The AVIRIS-NG image itself also suffers from different types of spatial and spectral errors (i.e., noise) that are common in hyperspectral imagery, although we removed noisy bands before performing the analyses.

It should also be noted that the feature compression on AVIRIS-NG images was conducted by RF-RFE model. With the development of deep-learning compression approaches (e.g., autoencoders) (La Grass et al. 2022), future research can compare their performance on reducing hyperspectral dimensionality while preserving spectral information in lichen mapping.

5. Conclusions

Caribou lichen fractional cover mapping is a challenging task over areas where non-lichen bright features (like rocks, sands, soil, etc.) are prevalent. Building on the hypothesis that in such areas the use of hyperspectral imagery would be advantageous, this study aimed to evaluate the use of AVIRIS-NG imagery to map Cladonia lichens in a rocky landscape shield in Canada. In this regard, we conducted a regression approach based on deep MLP models whose number of hidden layers and neurons were determined using exhaustive grid search procedures. According to our experiments, we observed some significant differences between the regression models trained on AVIRIS-NG image and the WV3 image. In most cases, the models trained on the AVIRIS-NG image resulted in higher R2 and lower RMSE values compared to the models trained on the WV3 image. However, even with the models trained on the AVIRIS-NG image, the accuracies of lichen fractional cover estimates were not high enough, at least compared to the results earlier reported using downscaled 6 m WV3 images for the same area (Fraser et al. 2021). Since this is the first study on the use of the AVIRIS-NG image for lichen fractional cover mapping in a complex landscape, there needs to be further work evaluating the potential of this imagery. For example, as a future work, one can consider incorporating other types of spatial information (like climate data, Digital Elevation Model (DEM) derivatives, etc.) into the workflow to analyse if these data can complement some of the gaps in AVIRIS-NG imagery for lichen mapping.

Acknowledgements

The authors would like to acknowledge Compute Canada and Google Colab for providing cloud computing platforms used for different analyses in this study. This study is funded as a part of the Government of Canada's initiative for monitoring and assessing regional cumulative effects, an added requirement to the new Impact Assessment Act (2019). It was also financially supported by National Science and Engineering Research Council (NSERC) Discovery grant and Queen's University Graduate Award.

References

Amarasingam, N., J. Sandin, A. Doshi, D. King, E. Blackman, J. Barthelemy, B. Bollard, S.A. Robinson, F. Gonzalez. 2025: Detection and mapping of Antarctic lichen using drones, multispectral cameras, and supervised deep learning. *International Journal of Applied Earth Observation and Geoinformation.* 141: 104577. doi.org/10.1016/j.jag.2025.104577

Ager, C. M., and N. M. Milton. 1987: Spectral reflectance of lichens and their effects on the reflectance of rock substrates. *GEOPHYSICS* 52 (7):898-906. doi: 10.1190/1.1442360.

Asta, J. et al. 2002: Mapping Lichen Diversity as an Indicator of Environmental Quality. In: Nimis, P.L., Scheidegger, C., Wolseley, P.A. (eds) Monitoring with Lichens — Monitoring Lichens. NATO Science Series, vol 7. Springer, Dordrecht. https://doi.org/10.1007/978-94-010-0423-7_19

Belgiu, M., and L. Drăguţ. 2016: Random Forest in remote sensing: A review of applications and future directions. *ISPRS Journal of Photogrammetry and Remote Sensing*, 114 (Supplement C):24-31. /doi.org/10.1016/j.isprsjprs.2016.01.011.

Falldorf, T., O. Strand, M. Panzacchi, and H. Tømmervik. 2014: Estimating lichen volume and reindeer winter pasture quality from Landsat imagery. *Remote Sensing of Environment*, 140:573-579. doi.org/10.1016/j.rse.2013.09.027.

Fraser, R. H., D. Pouliot, and J. van der Sluijs. 2021: UAV and High Resolution Satellite Mapping of Forage Lichen (Cladonia spp.) in a Rocky Canadian Shield Landscape. *Canadian Journal of Remote Sensing*:1-14. doi: 10.1080/07038992.2021.1908118.

Gilichinsky, M., P. Sandström, H. Reese, S. Kivinen, J. Moen, and M. Nilsson. 2011: Mapping ground lichens using forest inventory and optical satellite data. *International Journal of Remote Sensing*, 32 (2):455-472. doi: 10.1080/01431160903474962.

Hansen, M. J., S. E. Franklin, C. G. Woudsma, and M. Peterson. 2001: Caribou habitat mapping and fragmentation analysis using Landsat MSS, TM, and GIS data in the North Columbia

Mountains, British Columbia, Canada. *Remote Sensing of Environment*, 77 (1):50-65. doi: https://doi.org/10.1016/S0034-4257(01)00193-6.

He, L., W. Chen, S. G. Leblanc, J. Lovitt, A. Arsenault, I. Schmelzer, R. H. Fraser, R. Latifovic, L. Sun, C. Prévost, H. P. White, and D. Pouliot. 2021: Integration of multi-scale remote sensing data for reindeer lichen fractional cover mapping in Eastern Canada. *Remote Sensing of Environment* 267:112731. doi: https://doi.org/10.1016/j.rse.2021.112731.

Joly K, Cole M. J., and R. R. Jandt. 2007: Diets of overwintering Caribou, Rangifer tarandus, track decadal changes in Arctic Tundra vegetation. *Can. Field-Naturalist,* 121:379.

Joly, K., R. R. Jandt, and D. R. Klein. 2009: Decrease of lichens in Arctic ecosystems: the role of wildfire, caribou, reindeer, competition and climate in north-western Alaska. *Polar Research*, 28 (3):433-442. doi: 10.1111/j.1751-8369.2009.00113.x.

Jozdani, S., D. Chen, W. Chen, S. G. Leblanc, J. Lovitt, L. He, R. H. Fraser, and B. A. Johnson. 2021a: Evaluating Image Normalization via GANs for Environmental Mapping: A Case Study of Lichen Mapping Using High-Resolution Satellite Imagery. *Remote Sensing*, 13 (24). doi: 10.3390/rs13245035.

Jozdani, S., D. Chen, W. Chen, S. G. Leblanc, C. Prévost, J. Lovitt, L. He, and B. A. Johnson. 2021b: Leveraging Deep Neural Networks to Map Caribou Lichen in High-Resolution Satellite Images Based on a Small-Scale, Noisy UAV-Derived Map." *Remote Sensing*, 13 (14). doi: 10.3390/rs13142658.

Jozdani, S., D. Chen, D. Pouliot, and B. A. Johnson. 2022: A review and meta-analysis of generative adversarial networks and their applications in remote sensing. *International Journal of Applied Earth Observation and Geoinformation*, 108:102734. doi: https://doi.org/10.1016/j.jag.2022.102734.

Jozdani, S., A. B. Johnson, and D. Chen. 2019: Comparing Deep Neural Networks, Ensemble Classifiers, and Support Vector Machine Algorithms for Object-Based Urban Land Use/Land Cover Classification. *Remote Sensing*, 11 (14). doi: 10.3390/rs11141713.

Kennedy, B., D. Pouliot, M. Manseau, R. Fraser, J. Duffe, J. Pasher, W. Chen, and I. Olthof. 2020: Assessment of Landsat-based terricolous macrolichen cover retrieval and change analysis over caribou ranges in northern Canada and Alaska. *Remote Sensing of Environment*, 240:111694. doi: https://doi.org/10.1016/j.rse.2020.111694.

La Grassa R, Re C, Cremonese G, Gallo I. 2022: Hyperspectral Data Compression Using Fully Convolutional Autoencoder. Remote Sensing. 14(10):2472. https://doi.org/10.3390/rs14102472

Ma, L., Y. Liu, X. Zhang, Y. Ye, G. Yin, and B. A. Johnson. 2019: Deep learning in remote sensing applications: A meta-analysis and review. *ISPRS Journal of Photogrammetry and Remote Sensing*, 152:166-177. doi: https://doi.org/10.1016/j.isprsjprs.2019.04.015.

Macander, M. J., E. C. Palm, G. V. Frost, J. D. Herriges, P. R. Nelson, C. Roland, K. L. M. Russell, M. J. Suitor, T. W. Bentzen, K. Joly, S. J. Goetz, and M. Hebblewhite. 2020: Lichen cover mapping for caribou ranges in interior Alaska and Yukon. *Environmental Research Letters*. doi: 10.1088/1748-9326/ab6d38.

Miller, C. E., R. O. Green, D. R. Thompson, A. K. Thorpe, M. Eastwood, I. B. McCubbin, W. Olson-duvall, M. Bernas, C. M. Sarture, S. Nolte, L. M. Rios, M. A. Hernandez, B. D. Bue, and S. R. Lundeen. 2018: ABoVE: Hyperspectral Imagery from AVIRIS-NG, Alaskan and Canadian Arctic, 2017-2019. ORNL Distributed Active Archive Center.

Nordberg, M.-L.. 1998: Vegetation and biomass changes in mountainous areas in Sweden using satellite and airborne imaging scanner data. *27th International Symposium on Remote Sensing of Environment, Proceedings*, Tromso, Norway.

Nordberg, M.-L., and A. Allard. 2002: A remote sensing methodology for monitoring lichen cover. *Canadian Journal of Remote Sensing,* 28 (2):262-274. doi: 10.5589/m02-026.

Palmroos, I., V. Norros, S. Keski-Saari, et al. 2023: Remote sensing in mapping biodiversity – A case study of epiphytic lichen communities. Forest Ecology and Management. 538: 120993. https://doi.org/10.1016/j.foreco.2023.120993

Petzold, D. E., and S. N. Goward. 1988: Reflectance spectra of subarctic lichens. *Remote Sensing of Environment*, 24 (3):481-492. doi: https://doi.org/10.1016/0034-4257(88)90020-X.

Pinho, P., Augusto, S., Branquinho, C. et al. 2004: Mapping Lichen Diversity as a First Step for Air Quality Assessment. J Atmos Chem 49, 377–389. https://doi.org/10.1007/s10874-004-1253-4

Pouliot, D., N. Alavi, S. Wilson, J. Duffe, J. Pasher, A. Davidson, B. Daneshfar, and E. Lindsay. 2021: Assessment of Landsat Based Deep-Learning Membership Analysis for Development of from–to Change Time Series in the Prairie Region of Canada from 1984 to 2018. *Remote Sensing,* 13 (4). doi: 10.3390/rs13040634.

Richardson, G., S. G. Leblanc, J. Lovitt, K. Rajaratnam, and W. Chen. 2021: Leveraging AI to Estimate Caribou Lichen in UAV Orthomosaics from Ground Photo Datasets. *Drones*, 5 (3). doi: 10.3390/drones5030099.

Richardson, G., A. Knudby and W. Chen. 2023: Utilizing Transfer Learning with Artificial Intelligence for Scaling-Up Lichen Coverage Maps. *IGARSS 2023 - 2023 IEEE International Geoscience and Remote Sensing Symposium*, Pasadena, CA, USA, 2023, pp. 3050-3053, doi: 10.1109/IGARSS52108.2023.10283197.

Riihimäki, H., M. Luoto, and J. Heiskanen. 2019: Estimating fractional cover of tundra vegetation at multiple scales using unmanned aerial systems and optical satellite data. *Remote Sensing of Environment,* 224:119-132. doi: https://doi.org/10.1016/j.rse.2019.01.030.

Scheffler, D., A. Hollstein, H. Diedrich, K. Segl, and P. Hostert. 2017: AROSICS: An Automated and Robust Open-Source Image Co-Registration Software for Multi-Sensor Satellite Data. *Remote Sensing*, 9 (7). doi: 10.3390/rs9070676.

Théau, J., and C. R. Duguay. 2004: Lichen mapping in the summer range of the George River caribou herd using Landsat

TM imagery. *Canadian Journal of Remote Sensing*, 30 (6):867-881. doi: 10.5589/m04-047.

Yuan, Q., H. Shen, T. Li, Z. Li, S. Li, Y. Jiang, H. Xu, W. Tan, Q. Yang, J. Wang, J. Gao, and L. Zhang. 2020: Deep learning in environmental remote sensing: Achievements and challenges. *Remote Sensing of Environment*, 241:111716. doi: https://doi.org/10.1016/j.rse.2020.111716.

Zhang, J., B. Rivard, and A. Sánchez-Azofeifa. 2005: Spectral unmixing of normalized reflectance data for the deconvolution of lichen and rock mixtures. *Remote Sensing of Environment,* 95 (1):57-66. doi: https://doi.org/10.1016/j.rse.2004.11.019.